



Cite this: *Chem. Sci.*, 2025, **16**, 13715

All publication charges for this article have been paid for by the Royal Society of Chemistry

Received 8th April 2025  
Accepted 24th June 2025

DOI: 10.1039/d5sc02619a  
[rsc.li/chemical-science](http://rsc.li/chemical-science)

## Introduction

Biological systems are characterized by their precise regulation of chemical processes, energy production, and cellular homeostasis. A key component of these is the regulation of intracellular ion concentrations, which is achieved through naturally occurring ion channels and pumps, which in turn are tightly regulated by external stimuli such as small molecules, membrane potential and light.<sup>1</sup> Indeed, the malfunction of ion transport proteins is associated with life-threatening diseases, such as cystic fibrosis, which arises from misregulated chloride transport.<sup>2</sup> As such, synthetic supramolecular anionophores<sup>3</sup> have attracted significant interest as novel treatments for these diseases, as well as for potential cancer therapeutics.<sup>4-8</sup> However, coupling anion transport activity in these systems with stimulus-responsive control for spatio-temporal targeted applications, as is the case for biological systems, remains rare.<sup>9</sup> Multi-stimuli control offers the potential for tighter regulation of activity, but examples of this are rarer still.<sup>10-13</sup> Whilst systems controlled by light,<sup>14-23</sup> pH,<sup>24-27</sup> enzymes,<sup>13,28</sup> redox<sup>29-32</sup> and

membrane potential<sup>33</sup> have been reported, achieving high levels of control to switch between fully inactive “OFF” states and ion-transporting “ON” states is particularly challenging.

Reversibly gated ionophores based on azobenzene and stilbene photoswitches may exhibit background transport activities because of incomplete photoconversion between the two isomers.<sup>29</sup> Reversibly gated systems based on acylhydrazone and phenylhydrazone photoswitches have been developed by Talukdar and coworkers, and possess metastable states stabilized by intramolecular hydrogen bonding of the *Z* isomer.<sup>11,12</sup> However, the use of an exogenous acid input for activation is highly undesirable for biological contexts.

Irreversibly-gated systems can provide very effective OFF-ON control over ion transport activity. Examples include the use of photo-responsive cages to block anion binding sites in anion carriers,<sup>34,35</sup> control the self-assembly behaviour of channel-forming transporters,<sup>36</sup> or control anionophore lipid bilayer membrane mobility.<sup>37</sup> Other similar caged systems include the use of chalcogen bonding anionophores,<sup>31,38</sup> Au(III) caged systems,<sup>30</sup> and enzyme-responsive carriers.<sup>28</sup> Recently, we developed new approaches for controlling the transport activity utilizing caged anionophores.<sup>13,39</sup> In these transporters, a caged OFF state features amide protons that are locked through intramolecular hydrogen bonding and unavailable for anion binding, while decaging using light, redox, or enzymes renders them available for anion binding and therefore transport. Although these systems were found to be effective in terms of

<sup>a</sup>Chemistry Research Laboratory, Department of Chemistry, University of Oxford, 12 Mansfield Road, Oxford, OX1 3TA, UK. E-mail: matthew.langton@chem.ox.ac.uk

<sup>b</sup>Yusuf Hamied Department of Chemistry, University of Cambridge, Lensfield Road, Cambridge CB2 1EW, UK

† Electronic supplementary information (ESI) available. See DOI: <https://doi.org/10.1039/d5sc02619a>



their excellent OFF-ON activation behaviour, they lack a reversibly controlled response.

Despite the significant recent progress in the field of stimuli-controlled anionophore activity, one biological strategy that remains unexplored in the context of controllable synthetic ion carriers is that of competitive inhibition. Indeed, this highly effective mechanism allows for precise, reversible and controlled activity of ion transporters in nature. This approach has been exploited for the development of numerous therapeutics targeting ion channels, for example, those to treat heart arrhythmias by inhibiting cardiac sodium channels,<sup>40</sup> and a handful of synthetic ion channels gated by ligand binding have been reported.<sup>41-47</sup> We envisaged that competitive inhibition could conceivably be applied to anionophore design, wherein the addition of a correctly designed inhibitor forms a stable complex with the anion carrier, thereby blocking and turning 'OFF' anion transport activity.

Herein, we report a gated anion carrier transport system based on a Hamilton receptor<sup>48</sup> incorporating a hydrogen bond switch mechanism, utilising both photo-activation and an unprecedented competitive inhibition mechanism to control its activity (Fig. 1). Caging of the hydroxy groups of the Hamilton receptor with *ortho*-nitrobenzyl (ONB) group inhibits anion transport by locking amide protons through intramolecular hydrogen-bonding. Decaging of ONB groups using light reverses the hydrogen bonding pattern, rendering amide N-H protons available for anion binding and transport. The transport activity can be subsequently turned OFF using a barbiturate ligand as an external stimulus, which

competitively binds to the Hamilton receptor through multiple intermolecular hydrogen bonding interactions, thus inhibiting anion binding and transport.

## Results and discussion

### Design of the stimuli-responsive transporter platform

We identified a 4,6-dihydroxy-based Hamilton receptor as the key building block for the responsive anionophore platform (Fig. 1B). The Hamilton receptor provides the necessary 4,6-dihydroxy-isophthalamide core for anion binding and its transport across the lipid bilayer membrane, while pre-organization *via* intramolecular hydrogen bonding between the hydroxyl hydrogen bond donors and the adjacent carbonyl groups was expected to enhance anion binding and transport. Alkylation of these hydroxy groups in a 4,6-dihydroxy-isophthalamide anion receptor is known to disrupt this pattern, leading to an *anti-anti* arrangement of the amides and a decrease in anion binding affinity.<sup>49</sup> Ren and coworkers, and our group, have previously developed stimuli-responsive transport systems using a similar approach with alkyl-functionalized dihydroxy isophthalamide derivatives, in which photo-dealkylation of the hydroxyl groups generates the hydroxyl form, facilitating  $H^+$ / $Cl^-$  or  $NO_3^-$ / $Cl^-$  transport across lipid bilayer membranes.<sup>39,50,51</sup>

In our current work, we have targeted a Hamilton receptor derived from a 4,6-dihydroxy-isophthalamide scaffold as the key anionophore motif, which we anticipated would provide access to the corresponding *ortho*-nitrobenzyl (ONB) stimuli-

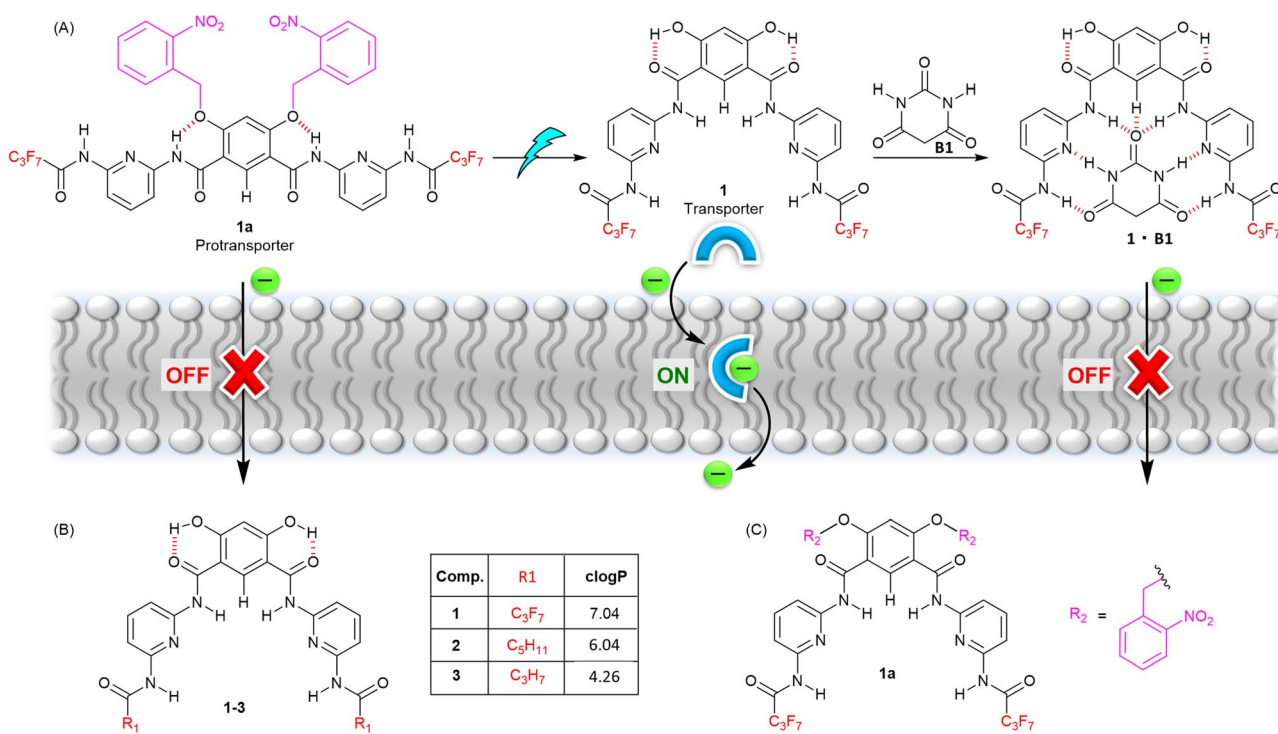


Fig. 1 (A) Schematic representation of stimuli-responsive anion transport. (B) Chemical structure of transporters **1-3**, with clogP values calculated using MarvinSketch. (C) Caged pro-transporter **1a**.



responsive pro-anionophore upon alkylation of the hydroxy groups with ONB moieties (Fig. 1C). Subsequent photodecaging would generate the active transporter, which could be deactivated again by competitive binding of a barbiturate ligand added as an external stimulus (Fig. 1A). Barbiturate ligands are known to bind to Hamilton receptors strongly through multiple intermolecular hydrogen bonding interactions.<sup>52,53</sup> Furthermore, varying the amide substitution of the Hamilton receptor's pyridine ring was expected to fine-tune the lipophilicities of the active transporters, in turn modulating their membrane permeabilities and therefore transport activities (Fig. 1B).

### Synthesis and anion binding experiments

To achieve the synthesis of the transporters **1–3**, 2,5-diaminopyridine **4** was converted into mono-amide derivatives **6a–6c** upon reacting with acyl chlorides **5a–5c**. Compounds **6a–6c** were coupled with di-benzylated isophthalic acid **7**,<sup>50</sup> to furnish debenzylated Hamilton receptor derivatives **8a–8c**. Finally, compounds **8a–8c** were debenzylated upon reaction with hydrogen in the presence of palladium on carbon to furnish the anionophores **1–3** in excellent yields (Fig. 2A).

To investigate the anion binding capabilities of compound **1**, <sup>1</sup>H NMR titration studies were performed in THF-*d*<sub>8</sub>. Addition of increasing equivalents of either tetrabutylammonium

chloride (TBACl) or tetrabutylammonium nitrate (TBANO<sub>3</sub>) to receptor **1** lead to downfield chemical shift of the amide N-H<sub>1</sub>, N-H<sub>3</sub> and C<sub>Ar</sub>-H<sub>2</sub> protons, respectively (Fig. 2C, S23 and S25<sup>†</sup>), indicative of N-H<sub>1</sub>···A<sup>–</sup>, N-H<sub>3</sub>···A<sup>–</sup>, and C<sub>Ar</sub>-H<sub>2</sub>···A<sup>–</sup> hydrogen bonding interactions and providing evidence for the pre-organised binding conformation (Fig. 2B). Analysis of the generated binding isotherms using Bindfit<sup>54</sup> determined the 1 : 1 host : guest association constant ( $K_{a(1:1)}$ ) of  $3087\text{ M}^{-1} \pm 10\%$  and ( $K_{a(1:1)}$ /NO<sub>3</sub><sup>–</sup>) of  $2639\text{ M}^{-1} \pm 8\%$ , respectively (Fig. 2D, S24 and S26<sup>†</sup>).

Anion binding studies could not be performed for receptors **2** and **3** because of their insolubility in THF-*d*<sub>8</sub> and other polar organic solvents. In addition to the chloride-induced chemical shift perturbations of H<sub>1</sub>, H<sub>2</sub> and H<sub>3</sub>, further evidence for the pre-organised conformation was obtained from <sup>1</sup>H-<sup>1</sup>H ROESY NMR spectroscopy in which through-space correlations were observed between protons H<sub>1</sub> and H<sub>2</sub> (Fig. S21<sup>†</sup>). This is consistent with previous studies highlighting the role of the intra-molecular hydrogen bonds in pre-organising such 4,6-dihydroxy-isophthalamide scaffolds, including crystallographic structural data of related systems.<sup>39,49</sup>

### Transmembrane ion transport experiments

The ion transport activities of the compounds **1–3** were evaluated using large unilamellar vesicles (LUVs) fluorescence assays.

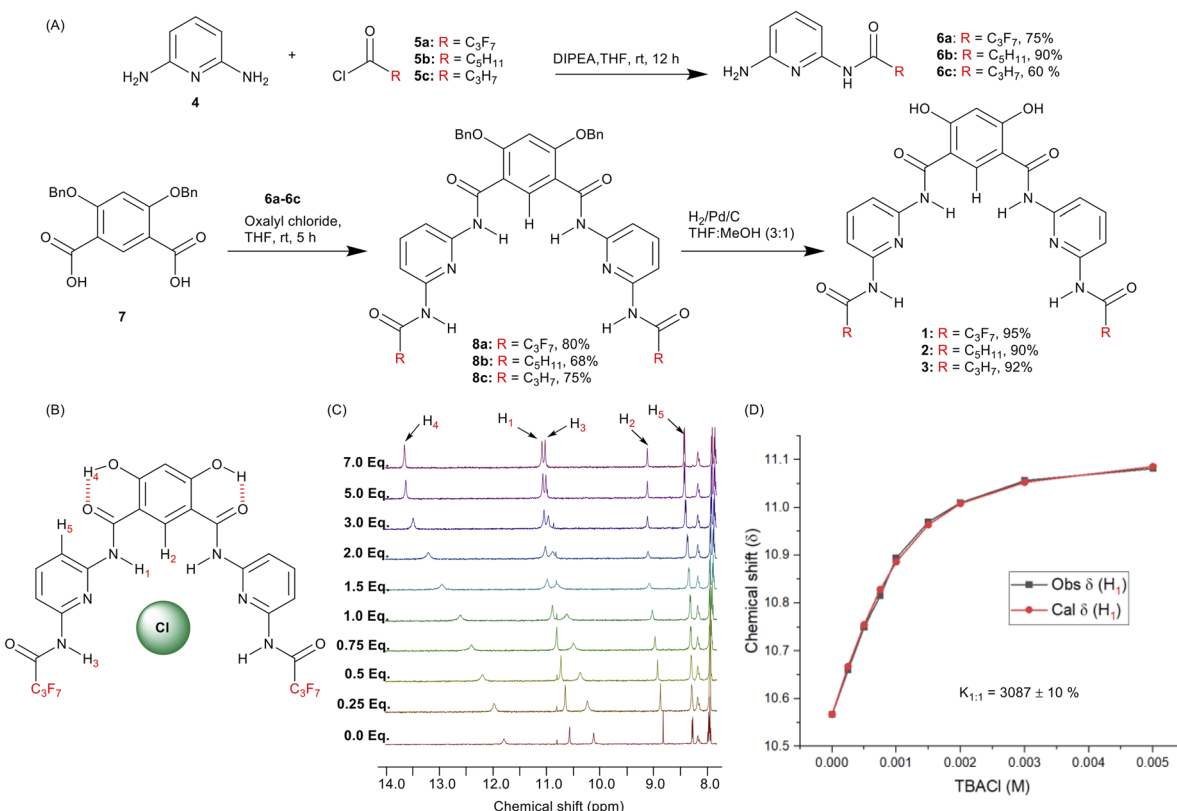


**Fig. 2** (A) Synthesis of transporters **1–3**. (B) Chemical structure of transporter **1** complexed to chloride. (C) <sup>1</sup>H NMR titration spectra for **1** (2.5 mM) in THF-*d*<sub>8</sub> with stepwise addition of TBACl in THF-*d*<sub>8</sub>. Protons assigned in panel B, and the equivalents of added TBACl are shown on the stacked spectra. (D) The plot of chemical shift (δ) of proton H<sub>1</sub> vs. concentration of TBACl added for transporter **1**, fitted to a 1 : 1 binding model using BindFit.



1-Palmitoyl-2-oleoyl-sn-glycero-3-phosphocholine vesicles (POPC LUVs) containing the pH-sensitive fluorophore 8-hydroxy pyrene-1,3,6-trisulfonic acid trisodium salt (HPTS, 1 mM) were prepared, containing 100 mM of NaCl and 10 mM HEPES buffer at pH 7. Subsequently, a pH gradient ( $\text{pH}_{\text{in}} = 7.0$  and  $\text{pH}_{\text{out}} = 7.8$ ) was created across the LUV membrane by the addition of a pulse of NaOH (5 mM) in the extravesicular solution. After addition of compounds **1–3**, the dissipation of the pH gradient through  $\text{OH}^-/\text{Cl}^-$  antiport (or the functionally equivalent  $\text{H}^+/\text{Cl}^-$  symport) was monitored by recording the change in fluorescence intensity at  $I_{\text{rel}}$  ( $\lambda_{\text{em}} = 510$  nm), with time following excitation at  $\lambda_{\text{ex}} = 405/465$ . At the end of each experiment, excess detergent (Triton X-100) was added to lyse the vesicles for calibration of the emission intensity. Significant ion transport was observed for all transporters with the activity sequence of **1** > **2** > **3**. The activity of the three transporters at 1.34 mol% loading (with respect to lipid) is shown in Fig. 3A, and the corresponding dose-response curves are given in the ESI (Fig. S29–S34†). Hill analysis furnished the  $EC_{50}$  values of  $0.032 \mu\text{M} \pm 0.002$  ( $0.096 \pm 0.005$  mol%) for **1**,  $7.1 \mu\text{M} \pm 0.4$  ( $22.9 \pm 0.1$  mol%) for **2**, and  $23.6 \mu\text{M} \pm 1.9$  ( $76.1 \pm 6.0$  mol%) for **3**, respectively. Hill coefficients ( $n$ ) were found to be  $\sim 1$  for all cases, suggesting the involvement of a 1:1 receptor–anion complex in the transmembrane anion transport process. The above activity sequences of **1** > **2** > **3** is most likely determined by

the varying lipophilicity of the transporters, as the substituents attached to fine-tune their lipophilicities are not anticipated to significantly affect the anion binding properties of these transporters. The compound **1** with the optimum clogP value furnishes the best transport activity.

Chloride transport by the best-performing transporter **1** was subsequently studied using lucigenin-based LUV assays. LUVs entrapping lucigenin – a fluorophore quenched by chloride – were prepared in 200 mM NaNO<sub>3</sub> buffered to pH 6.5 with 10 mM phosphate. Transporter **1** was then added in a 20  $\mu\text{L}$  aliquot of DMF at varying concentrations before a  $\text{Cl}^-/\text{NO}_3^-$  gradient was created by adding NaCl (33.3 mM) in the extravesicular buffer. The influx of chloride was evaluated by monitoring the rate of change in the fluorescence intensity ( $\lambda_{\text{ex}} = 455$  nm and  $\lambda_{\text{em}} = 535$  nm), and at the end of each experiment, excess detergent (Triton X-100) was added to lyse the vesicles for calibration of the emission intensity. Significant quenching was observed for the lucigenin after the addition of transporter **1**. The dose-dependent  $\text{Cl}^-$  influx by **1** is shown in Fig. 3D. Hill analysis furnished  $EC_{50}$  value of  $0.635 \pm 0.94 \mu\text{M}$  with a Hill coefficient value of  $\sim 1$ , consistent with that obtained in the above-mentioned HPTS pH dissipation experiments (Fig. S37†).

Mechanistically, the disruption of the pH gradient across the above POPC-LUVs  $\supset$  HPTS can occur through: (a)  $\text{H}^+/\text{X}^-$  symport, (b)  $\text{OH}^-/\text{X}^-$  antiport, (c)  $\text{H}^+/\text{M}^+$  antiport, or (d)  $\text{OH}^-/\text{M}^+$

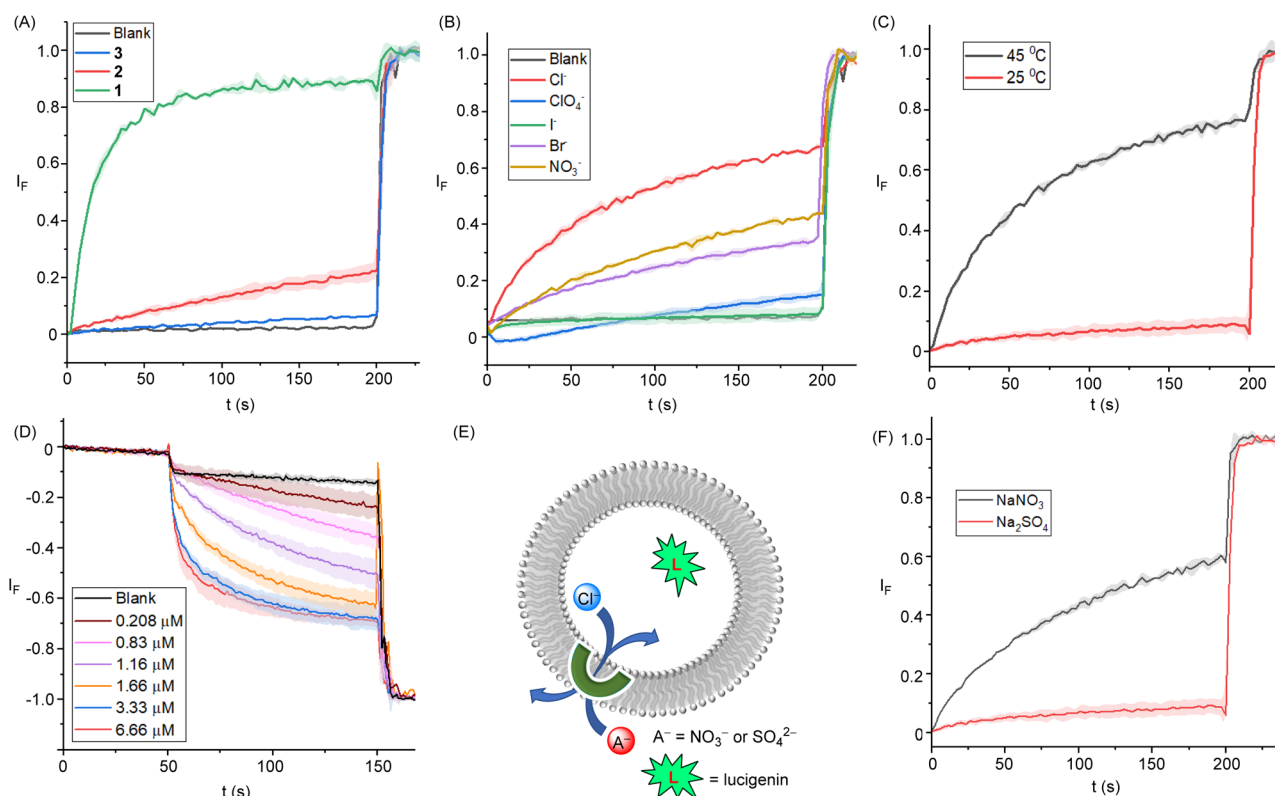


Fig. 3 (A) Ion transport activity comparison of **1–3** (1.34 mol%) across POPC-LUVs  $\supset$  HPTS. (B) Dependence of activity of **1** (0.193 mol%) on external anion  $\text{NaX}$  (where  $\text{X}^- = \text{Cl}^-, \text{Br}^-, \text{I}^-, \text{NO}_3^-, \text{and ClO}_4^-$ ). (C) Ion transport activity of **1** (0.33 mol%) across DPPC-based vesicles at 25 °C and 45 °C temperatures, respectively. (D) Ion transport activity of **1** across POPC-LUVs  $\supset$  lucigenin. (E) Schematic representation of chloride efflux with either extravesicular  $\text{SO}_4^{2-}$  and  $\text{NO}_3^-$  ions in the lucigenin assay. (F) Ion transport activity of **1** (3.0 mol%) in the presence of external  $\text{SO}_4^{2-}$  and  $\text{NO}_3^-$  ions.



symport transport modes. However, using intracellular NaCl and an iso-osmolar extravesicular  $M^+/Cl^-$  salt (where  $M^+ = Li^+, Na^+, K^+, Rb^+,$  and  $Cs^+$ ), no change in ion transport activity was observed, which rules out the possibility of  $H^+/M^+$  antiport and  $OH^-/M^+$  symport modes (Fig. S35†). Furthermore, changing the extravesicular  $Na^+/X^-$  salt ( $X^- = Cl^-, Br^-, I^-, NO_3^-$  and  $ClO_4^-$ ) resulted in significant modulation of the ion transport activity (Fig. 3B), demonstrating the role of anions in the overall transport process, and hence suggest that the ion transport process can occur through either  $OH^-/Cl^-$  antiport or  $H^+/Cl^-$  symport modes. Similarly, inactivity of the system when the chloride anions in the buffer were exchanged for gluconate – a large hydrophilic anion too hydrophilic to be transported – further confirmed that the transport in the presence of chloride is cation independent, occurring *via*  $Cl^-/OH^-$  antiport (or  $Cl^-/H^+$  symport) and not *via* a cation dependent  $H^+/Na^+$  antiport mechanism (Fig. S36†).

Finally, an antiport mode of transport was validated for  $Cl^-/NO_3^-$  exchange in the lucigenin-based fluorescence assays by exchanging the nitrate anion for the more hydrophilic dianionic sulfate. Lucigenin was encapsulated within the liposomes containing NaCl (200 mM) buffered at a pH of 6.5 with 10 mM phosphate. The ion transport activity was monitored in these LUVs suspended in either buffered  $NaNO_3$  (200 mM) or  $Na_2SO_4$  (200 mM). The transport activity was determined by recording the change in the lucigenin emission,  $I_f$  ( $\lambda_{em} = 535$  nm), with time following excitation at  $\lambda_{ex} = 460$  nm. Significant transport activity was observed in the presence of  $NaNO_3$ , which was absent in the presence of  $Na_2SO_4$  (Fig. 3F). The above results

suggest the  $Cl^-/NO_3^-$  antiport mode of ion transport dominates in this assay, rather than  $H^+/Cl^-$  symport, because in the latter no change in transport rates would be expected upon changing the anion, whilst for antiport, sulfate is highly hydrophilic and poorly transported compared to nitrate. Conducting analogous experiments in dipalmitoylphosphatidylcholine (DPPC) LUVs provided evidence for a mobile carrier mechanism. Inactivity at 25 °C, and restoration of activity at 45 °C, which is above the gel–liquid phase transition temperature for DPPC ( $T_m = 41$  °C), is indicative of a mobile carrier process, rather than transport mediated by self-assembly into an ion channel, the activity of which would be typically expected to be independent of the lipid phase (Fig. 3C).

### Synthesis and anion binding experiments of caged pro-transporter **1a**

Compound **1**, with optimum transport capabilities, was selected for caging with ONB photocleavable groups. Alkylation of **1** with 1-(bromomethyl)-2-nitrobenzene gave the corresponding light-responsive pro-transporter **1a** (Fig. 4A). Previous studies have demonstrated that such alkylation of the hydroxyl groups of the 4,6-dihydroxy-isophthalamide motif reverses the intra-molecular hydrogen bonding pattern, to adopt a conformation in which the amide NH protons interact with the ether O atoms, and are not available for anion binding.<sup>13,39,49</sup> Data suggesting **1a** adopts a similar conformation (Fig. 4A) was obtained from ROESY NMR and chloride binding titration experiments.  $^1H$ - $^1H$  ROESY interactions were observed between amide protons  $H_1$  and protons on the *ortho*-nitrobenzyl cages (Fig.

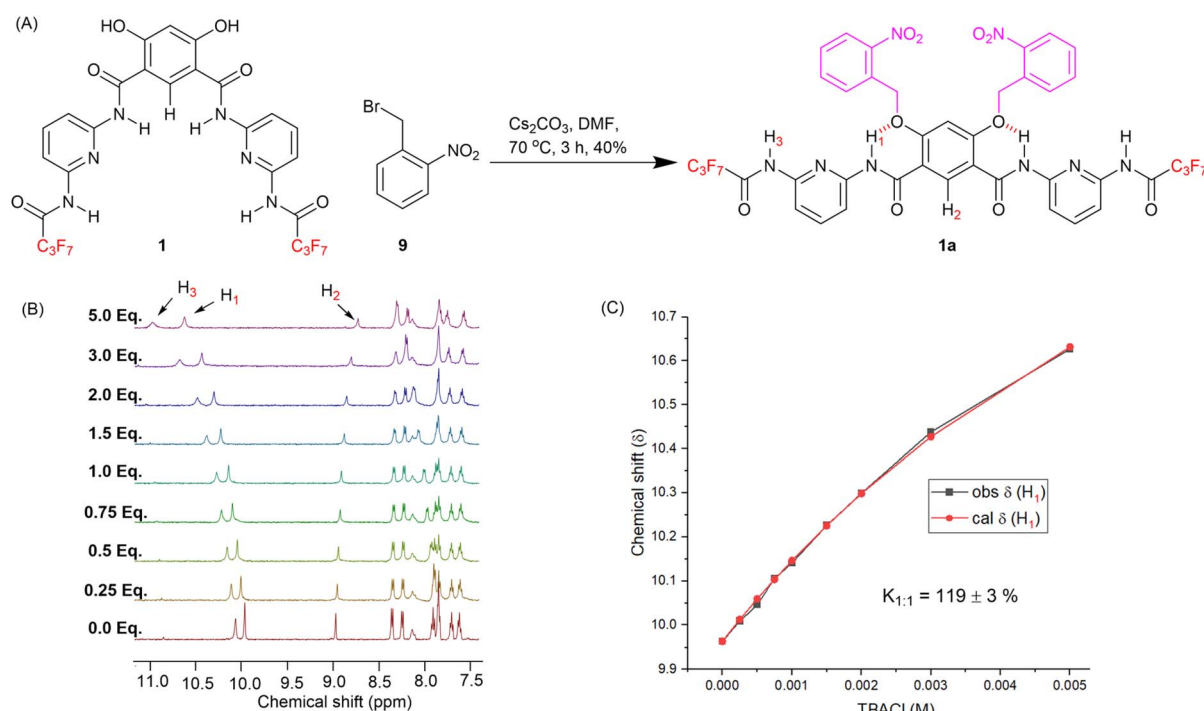


Fig. 4 (A) Synthesis of pro-transporter **1a**. (B)  $^1H$  NMR titration spectra for **1a** (2.5 mM in  $THF-d_8$ ) with stepwise addition of TBACl in  $THF-d_8$ . The equivalents of added TBACl are shown on the stacked spectra. (C) Plot of chemical shift ( $\delta$ ) of  $H_1$  proton vs. concentration of TBACl added for transporter **1**, and fit to a 1:1 binding model.



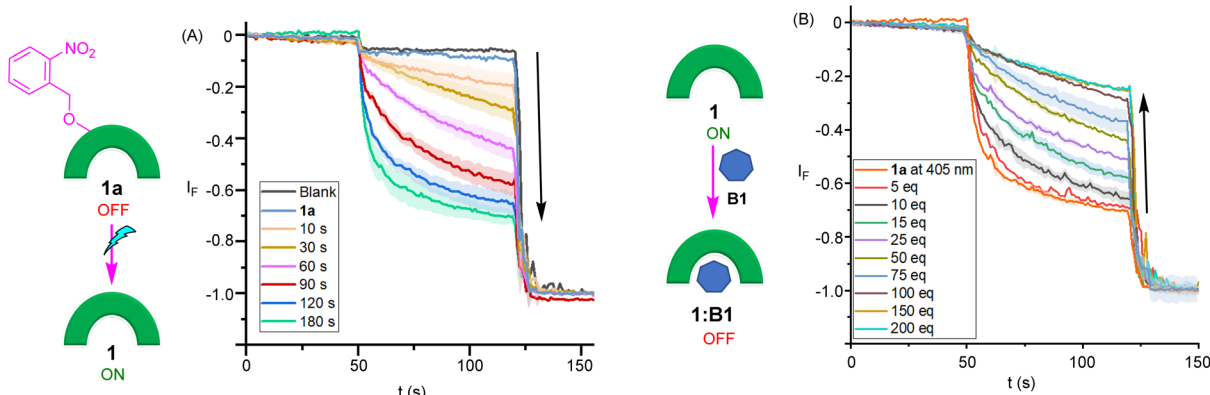


Fig. 5 (A) Ion transport activities across POPC-LUVs containing lucigenin after photo-irradiating **1a** at 405 nm light using an LED (1 W) and (B) treating **1a** with light for 5 minutes followed by the addition of barbiturate ligand **B1**.

**S22†**), as well as with  $\text{H}_2$ , confirming the proposed conformation with intra-molecular hydrogen bonding interactions is present in solution, and that the system is in dynamic equilibrium. A  $^1\text{H}$  NMR chloride binding titration experiment with **1a** in  $\text{THF}-d_8$  revealed minimal changes in the chemical shift of the amide protons upon addition of  $\text{TBACl}$  (Fig. 4B and S27†), which demonstrates the lack of chloride binding and suggests **1a** predominantly adopts the conformation with intra-molecular amide NH–O hydrogen bonds, which renders them less available for anion recognition. Using Bindfit, a 1 : 1 host–guest association constant ( $K_{\text{a}(1:1)}/\text{Cl}^-$ ) value of  $120 \text{ M}^{-1} \pm 3\%$  was determined (Fig. 4C and S28†), which is dramatically reduced compared to the association constant value of  $3087 \text{ M}^{-1} \pm 10\%$  for the preorganised, decaged transporter **1**.

### Stimuli-responsive ion transport experiments

Before proceeding to stimulus-responsive ion transport studies, photoactivation of pro-transporter **1a** and binding studies of transporter **1** with barbiturate ligands were performed in the solution phase. For **1a**, a 1 mM solution of the pro-transporter in  $\text{DMSO}-d_6$  was subjected to photoirradiation using a 405 nm LED and analysed by  $^1\text{H}$  NMR experiments. Complete decaging of **1a** to generate **1** was observed after 50 minutes of irradiation under these conditions (Fig. S40†). To monitor the binding of barbiturate ligand to Hamilton receptor **1**, UV-vis absorption studies were performed. Aliquots of barbiturate solution of **B1** (200 mM in DMF) were added to the receptor solution of **1** (6.6  $\mu\text{M}$  in DMF), and absorption spectra were recorded. Addition of barbiturate ligand **B1** to receptor **1** lead to a reduction in absorbance of the band at 363 nm corresponding to the free receptor, and an increase in absorbance at 320 nm corresponding to the host–guest complex (Fig. S42†). These changes confirmed the binding of the barbiturate ligand with the transporter molecule **1**. The data could be fitted to a 1 : 1 host–guest binding model, affording an association constant value of ( $K_{(1:1)}/\text{B1}$ ) =  $141 \text{ M}^{-1} \pm 5\%$  (Fig. S43†). Titration experiments with  $\text{TBACl}$  revealed that the analogous  $\text{Cl}^-$  association constant in DMF is approximately one order of magnitude lower ( $K_{\text{a}(1:1)}/\text{Cl}^- = 9 \text{ M}^{-1} \pm 14\%$ , Fig. S44 and S45†).

With evidence of efficient activation of pro-transporter **1a** to provide **1**, as well as barbiturate ligand binding to transporter **1** in the solution phase in hand, stimulus-responsive OFF–ON transport was evaluated using lucigenin-containing LUVs in phosphate buffered  $\text{NaNO}_3$  solution. Pro-transporter **1a** was added in an aliquot of DMF (final concentration of 3.0 mol% with respect to lipid), followed by adding  $\text{NaCl}$  (33.3 mM) in the extravesicular buffer to generate a  $\text{Cl}^-/\text{NO}_3^-$  gradient. No significant changes were observed in the lucigenin fluorescence, indicating that the pro-transporter **1a** is inactive at this concentration, consistent with results from  $^1\text{H}$  NMR chloride binding experiments, thus achieving an effective OFF state. Pro-transporter **1a** in phosphate buffered  $\text{NaNO}_3$  solution in a cuvette was then subjected to irradiation with a 1 W 405 nm LED, before adding LUVs and initiating ion transport by the addition of a chloride pulse. Photo-activation of **1a** (3.0 mol%) resulted in efficient activation, achieving comparable activity to a sample of **1** after 180 s of irradiation, indicative of near quantitative decaging under these conditions (Fig. 5A). For deactivation, **1a** (3.0 mol%) was initially photo-irradiated in the phosphate buffered  $\text{NaNO}_3$  solution with the 405 nm LED for 5 minutes to generate **1**, and subsequently barbiturate **B1** in DMF was added in with increasing equivalents and ion transport activity was monitored. Addition of barbiturate ligand **B1** (5–200 eq.) led to the significant deactivation of the ion transport (Fig. 5B). This deactivation was attributed to host–guest complex formation between the transporter **1** and the barbiturate ligand which results in the blockage of the anion binding cavity and stops the ion transport activity. To the best of our knowledge, this represents the first example of competitive inhibition of an ionophore by ligand binding.

### Conclusions

In conclusion, we have developed stimulus-responsive anion transporters based on hydrogen bonding interactions of hydroxyl-functionalised Hamilton receptor-based anionophores. Caging of the hydroxyl groups with light-responsive *ortho*-nitrobenzyl (ONB) causes the receptor to adopt



a conformation in which the amide NH protons form intramolecular interactions with the benzyl-ether O atoms, rendering them unavailable for anion binding and transport. Decaging with light reverses the hydrogen bonding pattern, such that the amide protons are available for anion binding and anion transport. The ion transport activity could be turned off again upon competitive binding of a barbiturate ligand to the Hamilton-receptor binding cavity. The combination of light and small molecule ligand binding thus provides a dual stimuli-responsive system enabling OFF-ON-OFF control over transport using an unprecedented competitive inhibition mechanism to regulate the anionophore activity.

## Data availability

All data supporting the findings of this study are available within the article and ESI.†

## Author contributions

M. A. performed the synthesis and characterization of the compounds, as well as the anion binding and transport studies and stimuli-responsive investigations. A. D. performed the synthesis and characterization of some of the compounds. M. A. wrote the first draft of the manuscript, which was edited by all authors. M. J. L. supervised the project.

## Conflicts of interest

There are no conflicts to declare.

## Acknowledgements

M. A. and M. J. L. acknowledge the Leverhulme Trust (RPG-2020-130) for financial support. M. A., A. D., and M. J. L. acknowledge funding from the Royal Society (RGF\EA\181007 and URF\R\231030). M. J. L. is a Royal Society University Research Fellow.

## Notes and references

- 1 B. Alberts, A. Johnson, J. Lewis, M. Raff, K. Roberts and P. Walter, *Molecular Biology of the Cell*, 4th edn, 2002.
- 2 J. Y. Choi, D. Muallem, K. Kiselyov, M. G. Lee, P. J. Thomas and S. Muallem, *Nature*, 2001, **410**, 94–97.
- 3 J. T. Davis, P. A. Gale and R. Quesada, *Chem. Soc. Rev.*, 2020, **49**, 6056–6086.
- 4 N. Busschaert, M. Wenzel, M. E. Light, P. Iglesias-Hernández, R. Pérez-Tomás and P. A. Gale, *J. Am. Chem. Soc.*, 2011, **133**, 14136–14148.
- 5 S. J. Moore, C. J. E. Haynes, J. González, J. L. Sutton, S. J. Brooks, M. E. Light, J. Herniman, G. J. Langley, V. Soto-Cerrato, R. Pérez-Tomás, I. Marques, P. J. Costa, V. Félix and P. A. Gale, *Chem. Sci.*, 2013, **4**, 103–117.
- 6 S.-K. Ko, S. K. Kim, A. Share, V. M. Lynch, J. Park, W. Namkung, W. Van Rossum, N. Busschaert, P. A. Gale, J. L. Sessler and I. Shin, *Nat. Chem.*, 2014, **6**, 885–892.
- 7 T. Saha, M. S. Hossain, D. Saha, M. Lahiri and P. Talukdar, *J. Am. Chem. Soc.*, 2016, **138**, 7558–7567.
- 8 N. Busschaert, S.-H. Park, K.-H. Baek, Y. P. Choi, J. Park, E. N. W. Howe, J. R. Hiscock, L. E. Karagiannidis, I. Marques, V. Félix, W. Namkung, J. L. Sessler, P. A. Gale and I. Shin, *Nat. Chem.*, 2017, **9**, 667–675.
- 9 M. J. Langton, *Nat. Rev. Chem.*, 2021, **5**, 46–61.
- 10 A. D. Peters, S. Borsley, F. Della Sala, D. F. Cairns-Gibson, M. Leonidou, J. Clayden, G. F. S. Whitehead, I. J. Vitórica-Yrezábal, E. Takano, J. Burthem, S. L. Cockcroft and S. J. Webb, *Chem. Sci.*, 2020, **11**, 7023–7030.
- 11 M. Ahmad, S. Chattopadhyay, D. Mondal, T. Vijayakanth and P. Talukdar, *Org. Lett.*, 2021, **23**, 7319–7324.
- 12 M. Ahmad, D. Mondal, N. J. Roy, T. Vijayakanth and P. Talukdar, *ChemPhotoChem*, 2022, e202200002.
- 13 M. Ahmad, T. G. Johnson, M. Flerin, F. Duarte and M. J. Langton, *Angew. Chem., Int. Ed.*, 2024, **63**, e202403314.
- 14 Y. R. Choi, G. C. Kim, H.-G. Jeon, J. Park, W. Namkung and K.-S. Jeong, *Chem. Commun.*, 2014, **50**, 15305–15308.
- 15 M. Ahmed, S. Metya, A. Das and P. Talukdar, *Chem. Eur. J.*, 2020, **26**, 8703–8708.
- 16 M. Ahmad, S. Sarkar, R. Bhogade, A. Mondal, D. Mondal, J. Mondal and P. Talukdar, *Nanoscale*, 2025, **17**, 3145–3151.
- 17 T. G. Johnson, A. Sadeghi-Kelishadi and M. J. Langton, *J. Am. Chem. Soc.*, 2022, **144**, 10455–10461.
- 18 A. Kerckhoffs and M. J. Langton, *Chem. Sci.*, 2020, **11**, 6325–6331.
- 19 W.-Z. Wang, L.-B. Huang, S.-P. Zheng, E. Moulin, O. Gavat, M. Barboiu and N. Giuseppone, *J. Am. Chem. Soc.*, 2021, **143**, 15653–15660.
- 20 A. Kerckhoffs, M. Ahmad and M. J. Langton, *Chem.-Eur. J.*, 2024, **30**, e202402382.
- 21 S. J. Wezenberg, L.-J. Chen, J. E. Bos, B. L. Feringa, E. N. W. Howe, X. Wu, M. A. Siegler and P. A. Gale, *J. Am. Chem. Soc.*, 2022, **144**, 331–338.
- 22 J. E. Bos, M. A. Siegler and S. J. Wezenberg, *J. Am. Chem. Soc.*, 2024, **146**, 31085–31093.
- 23 E. Grählert and M. J. Langton, *Angew. Chem., Int. Ed.*, 2024, e202421580.
- 24 E. N. W. Howe, N. Busschaert, X. Wu, S. N. Berry, J. Ho, M. E. Light, D. D. Czech, H. A. Klein, J. A. Kitchen and P. A. Gale, *J. Am. Chem. Soc.*, 2016, **138**, 8301–8308.
- 25 N. Busschaert, R. B. P. Elmes, D. D. Czech, X. Wu, I. L. Kirby, E. M. Peck, K. D. Hendzel, S. K. Shaw, B. Chan, B. D. Smith, K. A. Jolliffe and P. A. Gale, *Chem. Sci.*, 2014, **5**, 3617–3626.
- 26 A. Roy, O. Biswas and P. Talukdar, *Chem. Commun.*, 2017, **53**, 3122–3125.
- 27 S. V. Shinde and P. Talukdar, *Angew. Chem., Int. Ed.*, 2017, **56**, 4238–4242.
- 28 Y. R. Choi, B. Lee, J. Park, W. Namkung and K.-S. Jeong, *J. Am. Chem. Soc.*, 2016, **138**, 15319–15322.
- 29 M. Ahmad, S. A. Gartland and M. J. Langton, *Angew. Chem., Int. Ed.*, 2023, **62**, e202308842.
- 30 M. Fares, X. Wu, D. Ramesh, W. Lewis, P. A. Keller, E. N. W. Howe, R. Pérez-Tomás and P. A. Gale, *Angew. Chem., Int. Ed.*, 2020, **59**, 17614–17621.
- 31 B. Zhou and F. P. Gabbaï, *Chem. Sci.*, 2020, **11**, 7495–7500.



32 A. Docker, T. G. Johnson, H. Kuhn, Z. Zhang and M. J. Langton, *J. Am. Chem. Soc.*, 2023, **145**, 2661–2668.

33 X. Wu, J. R. Small, A. Cataldo, A. M. Withecombe, P. Turner and P. A. Gale, *Angew. Chem., Int. Ed.*, 2019, **58**, 15142–15147.

34 S. B. Salunke, J. A. Malla and P. Talukdar, *Angew. Chem., Int. Ed.*, 2019, **58**, 5354–5358.

35 M. Ahmad, N. J. Roy, A. Singh, D. Mondal, A. Mondal, T. Vijayakanth, M. Lahiri and P. Talukdar, *Chem. Sci.*, 2023, **14**, 8897–8904.

36 C. Bao, M. Ma, F. Meng, Q. Lin and L. Zhu, *New J. Chem.*, 2015, **39**, 6297–6302.

37 L. E. Bickerton and M. J. Langton, *Chem. Sci.*, 2022, **13**, 9531–9536.

38 G. Park and F. P. Gabbaï, *Chem. Sci.*, 2020, **11**, 10107–10112.

39 M. Ahmad, M. Flerin, H. M. Tay, A. L. Thompson, F. Duarte and M. J. Langton, *Nanoscale*, 2024, **16**, 21545–21553.

40 E. Ramos and M. E. O’Leary, *J. Physiol.*, 2004, **560**, 37–49.

41 V. Gorteau, F. Perret, G. Bollot, J. Mareda, A. N. Lazar, A. W. Coleman, D. H. Tran, N. Sakai and S. Matile, *J. Am. Chem. Soc.*, 2004, **126**, 13592–13593.

42 P. Talukdar, G. Bollot, J. Mareda, N. Sakai and S. Matile, *Chem. Eur. J.*, 2005, **11**, 6525–6532.

43 M. M. Tedesco, B. Ghebremariam, N. Sakai and S. Matile, *Angew. Chem., Int. Ed.*, 1999, **38**, 540–543.

44 T. Muraoka, T. Shima, T. Hamada, M. Morita, M. Takagi, K. V. Tabata, H. Noji and K. Kinbara, *J. Am. Chem. Soc.*, 2012, **134**, 19788–19794.

45 C. P. Wilson and S. J. Webb, *Chem. Commun.*, 2008, 4007–4009.

46 M. Boccalon, E. Iengo and P. Tecilla, *J. Am. Chem. Soc.*, 2012, **134**, 20310–20313.

47 C. J. E. Haynes, J. Zhu, C. Chimerel, S. Hernández-Ainsa, I. A. Riddell, T. K. Ronson, U. F. Keyser and J. R. Nitschke, *Angew. Chem., Int. Ed.*, 2017, **56**, 15388–15392.

48 S. K. Chang and A. D. Hamilton, *J. Am. Chem. Soc.*, 1988, **110**, 1318–1319.

49 P. V. Santacroce, J. T. Davis, M. E. Light, P. A. Gale, J. C. Iglesias-Sánchez, P. Prados and R. Quesada, *J. Am. Chem. Soc.*, 2007, **129**, 1886–1887.

50 Q. Zhong, Y. Cao, X. Xie, Y. Wu, Z. Chen, Q. Zhang, C. Jia, Z. Wu, P. Xin, X. Yan, Z. Zeng and C. Ren, *Angew. Chem., Int. Ed.*, 2024, **63**, e202314666.

51 M. Ahmad, A. Muir and M. J. Langton, *ACS Omega*, 2024, **9**, 45572–45580.

52 A. Tron, M. Rocher, P. J. Thornton, J. H. R. Tucker and N. D. McClenaghan, *Asian J. Org. Chem.*, 2015, **4**, 192–202.

53 S. Adhikari, A. Datta, I. Saha and K. Ghosh, *Coord. Chem. Rev.*, 2024, **517**, 215989.

54 <http://app.supramolecular.org/bindfit/>.

